2018 IEEE-RAS 18th International Conference on Humanoid Robots (Humanoids)
Beijing, China, November 6-9, 2018

Downsizing the Motors of a Biped Robot Using a Hydraulic Direct Drive System

J. Shimizu, T. Otani, K. Hashimoto, A. Takanishi, *Member, IEEE*

***Abstract*— Biped robots require a high power to be provided alternately on their two legs while walking, hopping, and running. However, the mounting of high-power and large electrical motors is challenging in conventional mechanical transmission systems because of space limitations. To address this issue, we employ herein a combination of hydraulic and transmission systems with an independent driving mode and a power-shared driving mode. In the independent driving mode, an actuator can be independently controlled based on flow-control, and pressure loss can be reduced. In the power-shared driving mode, actuators can also be controlled based on flow-control, and this mode allows the motor power of the left and right legs to be shared. We also employ a simulation to evaluate the proposed novel system and confirm that the motor power could be reduced by 35.6% for the hopping movement. This result shows that the rated output of the required motor can be reduced, and the selection of smaller and lighter motors is possible for installation in biped robots.**

I. Introduction

The safety and quantitative evaluation of products used by humans is required; however, a conventional user evaluation has safety risks and problem on reproducibility. Therefore, we propose herein the use of a biped humanoid robot to perform such evaluations. The robot named WABIAN-2R (WAseda BIpedal humANoid — No. 2 Refined) is capable of executing a stretched knee gait with a pelvis model [1]. We are developing robots with high exercise performance to evaluate the products used while walking, running, and hopping. However, in such a robot, high-power actuators are required, with the installation of high-power electric motors being difficult in human-sized robots because of space limitations. To resolve this issue, we proposed a method to generate a large torque by combining pelvic oscillation and leg elasticity [2, 3]. Figure 1 shows these biped robots.

*This study was conducted with the support of the Research Institute for Science and Engineering, Waseda University and Future Robotics Organization, Waseda University and as a part of the humanoid project at the Humanoid Robotics Institute, Waseda University. It was also financially supported in part by JSPS KAKENHI Grant No.17H00767. We would like to thank Editage (www.editage.jp) for the English language editing.

Juri Shimizu is with the Graduate School of Advanced Science and Engineering, Waseda University, and is a researcher at Hitachi, Ltd. (#41-304, 17 Kikui-cho, Shinjuku-ku, Tokyo 162-0044, Japan) (e-mail: contact@takanishi.mech.waseda.ac.jp)

Takuya Otani is with the Department of Modern Mechanical Engineering, Waseda University, and is a researcher at the Humanoid Robotics Institute (HRI), Waseda University.

Kenji Hashimoto is with the School of Science and Technology, Meiji University, and is a researcher at the Humanoid Robotics Institute, Waseda University.

Atsuo Takanishi is with the Department of Modern Mechanical Engineering, Waseda University, and is the director of the Humanoid Robotics Institute, Waseda University.

As a means to realize a small and high-power motor, Urata et al. reported a technique that uses a liquid cooling system to improve the continuous output torque [4]. Other robots, in which two motors are mounted in the driving axes, have also been reported [5, 6]. Although these approaches have achieved a highly mobile humanoid with high speed and high torque joints in both legs, the difference here is that high-power actuators are alternately (rather than simultaneously) required for cyclic motions, such as walking, running, and hopping. In the conventional methods described earlier, the motor outputs can be used only for each axis because they are directly connected to the axes by the mechanical transmission. Thus, the size of the motor can be further reduced if the output of the driving source of both legs can be shared.

Hydraulic systems can share the output of the drive source. For example, Boston Dynamics showed the hydraulic humanoid robot, ATLAS [7], while Hyon et al. demonstrated the capabilities of TaeMu [8]. Although these robots control each axis with proportional valves, these valves generate energy loss. A displacement control system has been suggested to reduce such hydraulic energy losses [9, 10]. This system was applied to the robot system of Kaminaga's electro-hydrostatic actuator [11]; however, the pumps were unable to share their output powers in such systems.

Thus, we propose herein a system for downsizing motors by sharing the outputs of the actuators of both legs to permit cyclic and symmetrical motions in biped robots. We consider a hydraulic drive system because it should be capable of sharing the output. By combining the outputs of the left and right motors, we expect that it will be possible to reduce the load of each motor, thereby allowing the selection of smaller and lighter motors for biped robots. We also apply flow-based control to the hydraulic system to minimize loss.

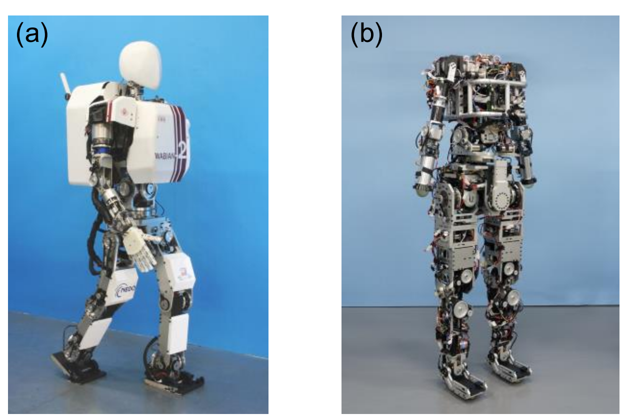

Figure 1. Examples of biped robots reported by our group. (a) The walking robot (WABIAN-2R [1]) and (b) the running robot [3].

978-1-5386-7282-2/18/$31.00 ©2018 IEEE

II. Development of the Hydraulic System And Control

A. Hydraulic Direct Drive System Circuit

We designed a hydraulic system that independently drives the axis of each leg and can share the power outputs between both legs.

For the hydraulic-based drive system described herein, we selected an actuator speed control based on the pump output flow to minimize valve loss. In addition, we selected a single-rod cylinder as a hydraulic actuator because this type of actuator is commonly used for hydraulic machines, such as excavators. A single-rod cylinder is generally more efficient than a hydraulic motor, and has better availability and mountability compared to a through-rod cylinder.

Furthermore, we selected a fixed displacement pump because this type of pump demonstrates a superior volumetric efficiency than a variable displacement pump. In the case of the fixed displacement pump, a displacement control unit is not required; hence, it is relatively small, and can be easily mounted. In this type of pump, the flow rate can be controlled by regulating the pump's rotational speed. Thus, in our case, the pump was connected to a servo motor, and the flow rate was controlled by regulating the rotational speed of the motor. Figure 2 shows the proposed hydraulic direct drive system for a single axis, where the pump and the cylinder are connected through Valve 1. Valve 1 is a solenoid direction-control valve. The pump outlet port is connected to the cap side of the cylinder (without the input signal to Valve 1) and connected to the rod side by the input signal. Therefore, Valve 1 can control the operating direction of the cylinder. In addition, the tank and the outlet side of the cylinder are connected through valves 1 and 2. Valve 2 is a solenoid proportional control valve, and the opening of Valve 2 can be controlled by an input signal. In this case, Valve 2 is used to control the actuator speed in the meter-out mode, as will be described later. Finally, a relief valve is connected to the pump outlet line to prevent the pump outlet pressure from exceeding the set pressure and ultimately prevent damage to the pump.

Thus, the circuit shown in Figure 2 was installed on both legs, and a circuit that connects the left and right systems was applied. Figure 3 depicts the proposed circuit. Valve 3 is located on the line connecting the left and right cylinders. This valve is a solenoid direction-control valve that constitutes the single-axis drive system (Figure 2) without an input signal. Valve 3 connects the left and right cylinders by an input signal. With this connection, the state of the valves determines the operating direction of the left and right cylinders. TABLE I lists the relationships between the states of valves 1 and 3 and the operating direction of the cylinder.

Figure 4 shows an example of the independent drive mode. The state shown corresponds to No. 3 listed in TABLE I. In Figure 4, the input signal of Valve 1 in the left leg side is OFF, and the input signal of the right leg side is ON.

The flow rate in the left leg side is provided to the cap side of the cylinder and drives it in the outstroke direction. The cylinder rod output flow is discharged to the tank through Valve 2. In contrast, the flow rate in the right leg side is provided to the rod side of the cylinder and drives it in the

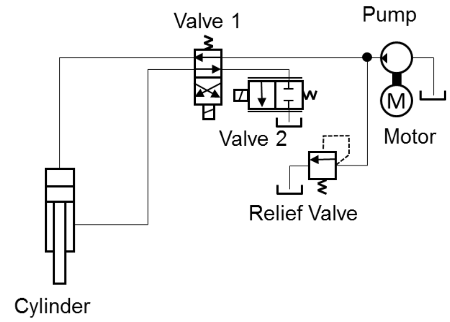

Figure 2. Proposed hydraulic direct drive circuit (single axis).

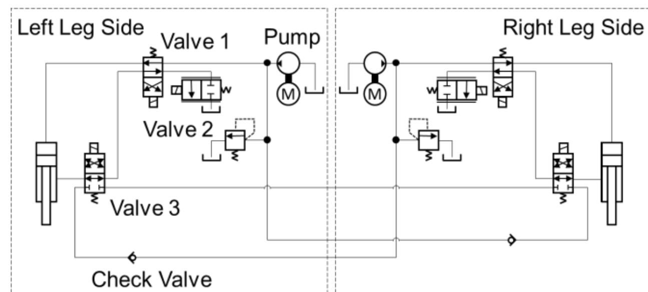

Figure 3. Proposed hydraulic direct drive circuit (double axis).

TABLE I. Valve Input Signals and Cylinder Directions

No.	Input signal				Direction	
	Valve 1		*Valve 3*		*Cylinder*	
	Left	*Right*	*Left*	*Right*	*Left*	*Right*
1	OFF	OFF	OFF		Outstroke	Outstroke
2	ON				Instroke	Outstroke
3	OFF	ON			Outstroke	Instroke
4	ON				Instroke	Instroke
5	OFF	ON	ON		Outstroke	Instroke
6	ON	OFF			Instroke	Outstroke

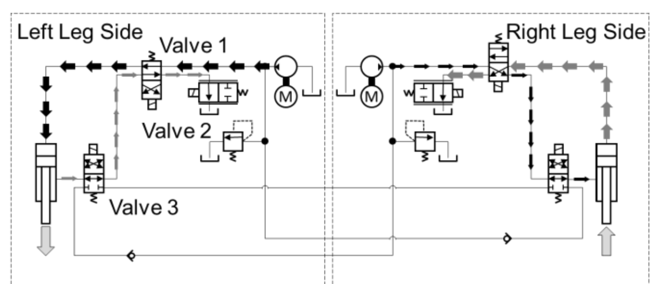

Figure 4. Independent driving mode.

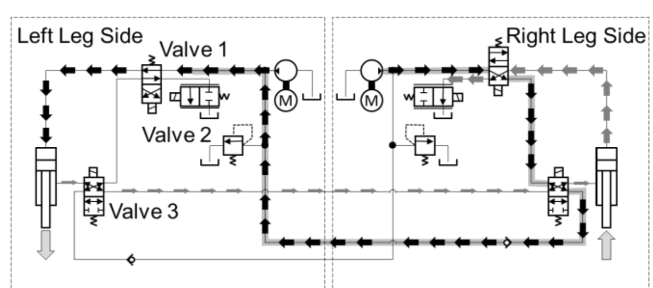

Figure 5. Power-shared driving mode.

instroke direction. The cylinder cap output flow is discharged to the tank through Valve 2. As described earlier, in the independent drive mode, the left and right pumps or Valve 2 can independently control the speeds of the left and right cylinders.

Figure 5 shows an example of the power-shared drive mode, where the state shown corresponds to No. 5 listed in TABLE I. In Figure 5, the input signals of Valve 3 are ON for both sides, and the signal of Valve 1 in the right leg side is ON. The pump output line in the right leg side is connected to the pump output line in the left leg side. The output flows derived from the two pumps are provided to the cap side of the cylinder in the left leg side and drive it in the outstroke direction. The cylinder rod output flow in the left leg side is then discharged to the cylinder rod in the right leg side through Valve 3, and the cylinder cap output flow in the right leg side is discharged to the tank through valves 1 and 2.

As described earlier, in the power-shared mode, the derived output flow can be input into a single cylinder, allowing the driving speed of the cylinder to be doubled in the independent drive mode. In other words, the cylinder can be driven with half the power of the independent drive mode ideally at the same speed. However, this effect is reduced by the efficiency of the pump and pressure loss within the circuit. Without the pump connection, the cylinder can also be driven at the same speed by the discharge flow rate of the cylinder with the pump connection. In a biped robot, considering cyclic and symmetrical motions, such as walking, hopping, and running, a high power is required for the stance leg side, and a low power is required for the swing leg side. In such an operational pattern, a reduction of the motor's output can be expected if the pump is connected to the stance leg side, and the swing leg side is driven with the output flow of the stance-side cylinder.

B. Control of the Hydraulic Direct Drive System

In the circuit shown in Figure 2, two different flow-control modes were applied depending on the external force acting on the cylinder and the driving direction.

More specifically, the first flow-control mode was a meter-in flow-control mode with a positive load, in which the driving direction of the cylinder and the direction of the external force were opposite. Figure 6(a) shows examples of the meter-in flow-control mode, where the chamber of the cylinder connected to the pump has a high pressure. In this state, the cylinder input flow rate is comparable to the pump derived output; thus, the pump can control the cylinder velocity.

The second control mode was a meter-out flow-control mode with a negative load, in which the driving direction of the cylinder and the direction of the external force were the same. Figure 6(b) show examples of the meter-out flow control, where a pressure is present in the chamber of the cylinder connected to Valve 2. In this state, the cylinder output flow

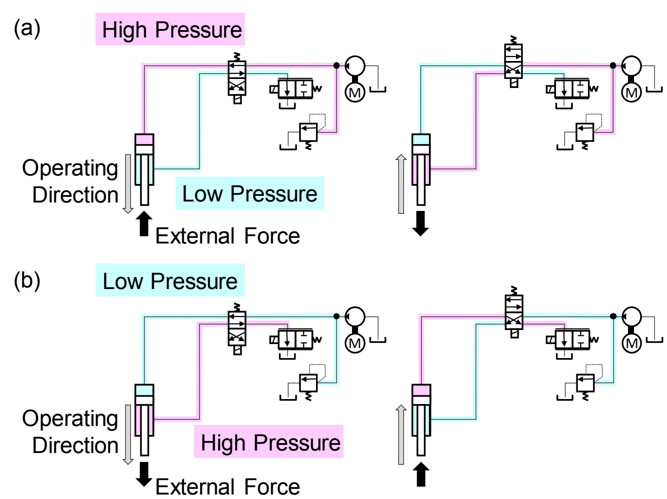

Figure 6. Flow-control modes: (a) meter-in mode and (b) meter-out mode.

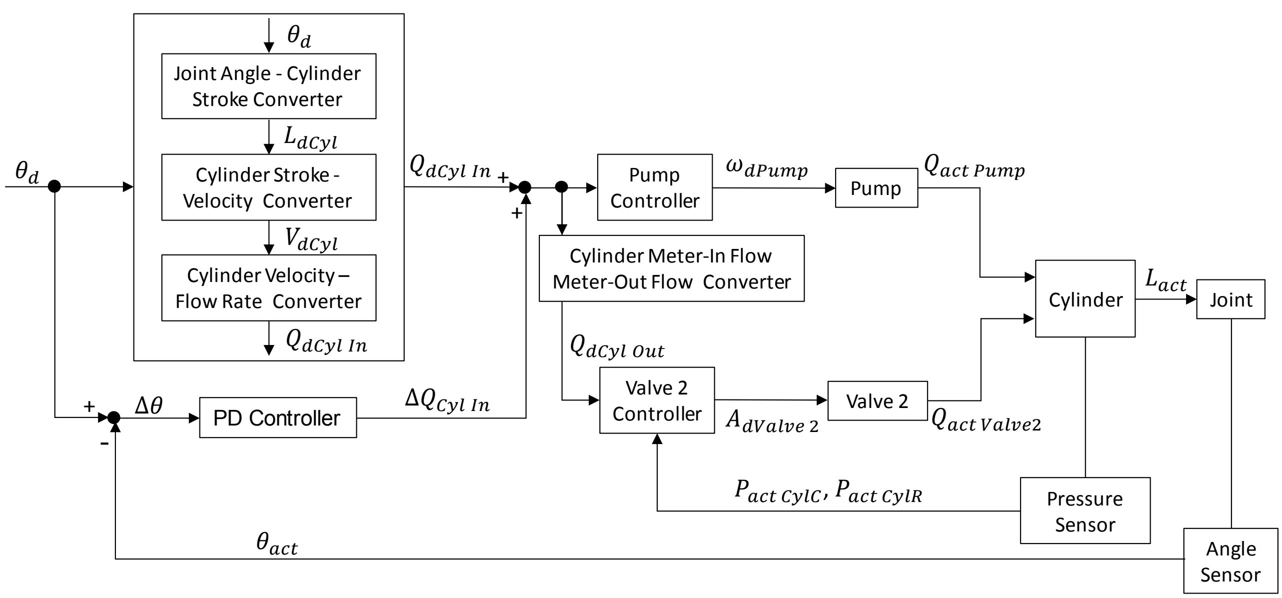

Figure 7. Block diagram of the flow-control.

rate is comparable to that of the Valve 2 flow rate; hence, this valve can control the cylinder velocity.

Figure 7 shows the block diagram of the flow-control. The input is the demand value of the joint angle θ_d, and the output is the actual value of the joint angle θ_{act}. In the proposed hydraulic system, the joint angle is driven by a cylinder. Where the four-bar link mechanism (described later) was employed, the length of the cylinder can be determined by the joint angle. Therefore, the demand stroke of the cylinder L_{dCyl} is calculated from the demand angle θ_d, and the demand velocity of the cylinder V_{dCyl} is calculated from the time variation amount of the demand stroke L_{dCyl}:

$$V_{dCyl} = \frac{dL_{dCyl}}{dt} \tag{1}$$

The cylinder meter-in flow rate $Q_{dCyl\,in}$ can be expressed as follows based on the demand velocity of the cylinder V_{dCyl}:

$$Q_{dCyl\,in} = \begin{cases} V_{dCyl}\,A_{CylCap}\,(V_{dCyl} > 0 : Outstroke) \\ V_{dCyl}\,A_{CylRod}\,(V_{dCyl} < 0 : Instroke) \end{cases} \tag{2}$$

where A_{CylCap} is the pressure receiving area of the cylinder on the cap side, and A_{Cylrod} is the pressure receiving area on the cap side.

The cylinder meter-in flow rate $Q_{dCyl\,in}$ is controlled by the pump derived output flow Q_{pump} in the meter-in flow-control mode. Q_{pump} is given by:

$$Q_{pump} = D_p\,\omega\,\eta_{pv} \tag{3}$$

where D_P is the displacement of the pump; ω is the rotational speed of the pump; and η_{pv} is the volumetric efficiency. In this system, we applied a fixed displacement pump that controlled its derived output flow Q_{pump} by its rotational speed ω. Therefore, the demand pump rotational speed ω_{dpump} can be determined from Equations (2) and (3):

$$\omega_{dpump} = \frac{V_{dCyl}\,A_{Cyl}}{D_p\ \eta_{pv}} \tag{4}$$

The cylinder meter-out flow rate $Q_{dCyl\,out}$ can be expressed as follows based on the cylinder meter-in flow rate $Q_{dCyl\,in}$:

$$Q_{dCyl\,out} = \begin{cases} \frac{A_{CylRod}}{A_{CylCap}}\,Q_{dCyl\,in}\,(V_{dCyl} > 0 : Outstroke) \\ \frac{A_{CylCap}}{A_{CylRod}}\,Q_{dCyl\,in}\,(V_{dCyl} < 0 : Instroke) \end{cases} \tag{5}$$

The cylinder meter-in flow rate $Q_{dCyl\,out}$ is controlled by the flow rate of the Valve 2 $Q_{Valve\,2}$ in the meter-out flow-control mode. $Q_{Valve\,2}$ is generally given by:

$$Q_{Valve\,2} = C_d\,A_{Valve\,2}\sqrt{\frac{2\,(P_{Valve\,2\,in} - P_{Valve\,2\,out})}{\rho}} \tag{6}$$

where C_d is the flow coefficient; $A_{Valve\,2}$ is the valve opening area; $P_{Valve\,2\,in}$ and $P_{Valve\,2\,out}$ are the pressures at the input port and the output port of Valve 2, respectively; and ρ is the fluid density. $P_{Valve\,out}$ is approximately 0, and $P_{Valve\,in}$ is comparable to the cylinder pressure of the meter-out side.

In an actual system, the demanded flow rate of the pump and the valve is not produced because of its leakage or a response delay. This flow rate error makes the error of the joint angle in the robot. Therefore, the correction flow rate $\Delta Q_{Cyl\,in}$ was calculated by the PD controller, which used the error between the demanded joint angle θ_d and the actual angle θ_{act}. Applying $\Delta Q_{Cyl\,in}$, ω_{dpump} can be expressed as:

$$\omega_{dpump} = \frac{V_{dCyl}\,A_{Cyl} + \Delta Q_{Cyl\,in}}{D_p\ \eta_{pv}} \tag{7}$$

Considering $\Delta Q_{Cyl\,in}$, $A_{dValve\,2}$ can be calculated using Equation (8):

$$A_{dValve\,2} = \frac{\alpha(Q_{dCyl\,in} + \Delta Q_{Cyl\,in})}{C_d}\sqrt{\frac{\rho}{2\,P_{act\,Cyl\,low}}} \tag{8}$$

The meter-in flow-control and the meter-out flow-control mode can also be applied in the power shared driving mode, and the control that is applied in this mode is determined from two pressures. More specifically, one of these pressures is the pressure of the cylinder chamber connected to the pumps, while the other is the pressure of the cylinder chamber connected to Valve 2 in the opposite side leg. For example, in Figure 5, these pressures are the cap pressure in the left leg side and the rod pressure in the right leg side.

III. Experimental Results

We initially conducted a simulation experiment to confirm the energy reduction by the hydraulic direct drive system for a mechanical transmission system. For this purpose, we used the LMS Imagine.Lab Amesim™ (Siemens K.K.) physical modeling tool to evaluate the hydraulic direct drive system.

A. Hopping Simulation of a Simple Model

We selected the one leg hopping operation as the motion in which the output concentrates on one leg to evaluate the effect of the proposed system.

In this context, a simple hopping model was demonstrated by Raibert [12] (Figure 8). This model was constrained to move on the X–Z plane; hence, no rotation was observed about the Y-axis. The point, where the ankle makes contact with the ground, is known as the grounding point.

Initially, the length of the right leg L_{R1} at the first hopping was changed according to a sine wave; hence, L_{R1} is given by:

$$L_{R1} = L_0 + \alpha_s \sin\omega_s t \tag{9}$$

where L_0 is the initial length of the legs; α_s is the amplitude; and ω_s is the input frequency. The time of flight is expressed as follows:

$$T_f = \frac{2\dot{Z}_f}{g} \tag{10}$$

where $\dot{Z}_f$ is the velocity at the release time. Subsequently, the length of the right leg L_{R2} during the second hopping was altered according to a sine wave. To achieve a smooth landing, L_L is given by:

$$L_{R2} = L_0 + \alpha_s \sin\omega_s(t - \phi_d) \tag{11}$$

where ϕ_d is the phase delay time, and:

$$\phi_d = T_f - 2\left(\frac{\pi}{2\omega_s} - \phi_f\right) \tag{12}$$

where ϕ_f represents the time from the initial length to the release time. In this simulation, the length of the left leg L_L was shorter than that of the right leg L_R to avoid contact with the ground. To achieve each required leg length L, the left and right hip joint angles θ_{hip}, the knee joint angles θ_{knee}, and the ankle joint angles θ_{ankle} can be expressed as follows:

$$\theta_{hip} = \cos^{-1}\frac{L/2}{l_{thigh}} \tag{13}$$

$$\theta_{knee} = 2\sin^{-1}\frac{L/2}{l_{thigh}} \tag{14}$$

$$\theta_{ankle} = \cos^{-1}\frac{L/2}{l_{shank}} \tag{15}$$

Upon landing, the ankle joint angle θ_{ankle} was corrected, such that the center of gravity position and the grounding point became a linear straight line to obtain stable hopping.

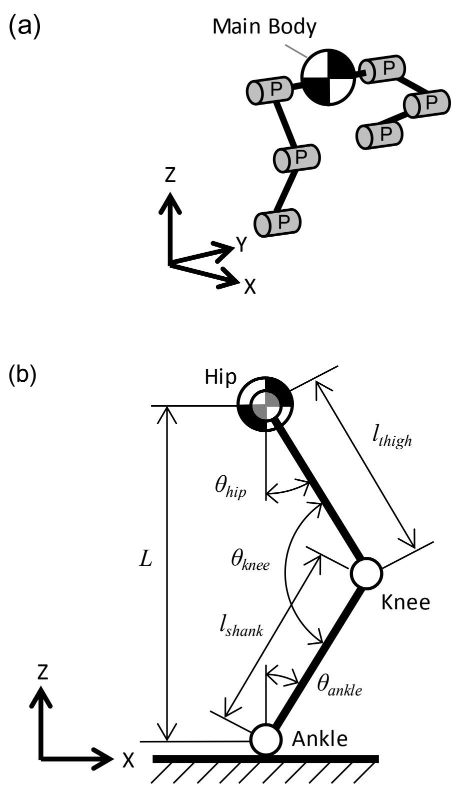

Figure 8. Simple hopping model: (a) degree of freedom configuration and (b) model parameters.

TABLE II. LEG MECHANICAL MODEL PARAMETERS

Thigh length (mm)	500
Thigh weight (kg)	1.0
Shank length (mm)	500
Shank weight (kg)	1.0
Main body weight (kg)	62.5

TABLE III. HOPPING CONTROL PARAMETERS

L_0 (mm)	940
ω_s (rad/s)	15.7
α_s (mm)	55

Figure 8 and TABLE II show the parameters of the mechanical model. TABLE III presents the hopping control parameters.

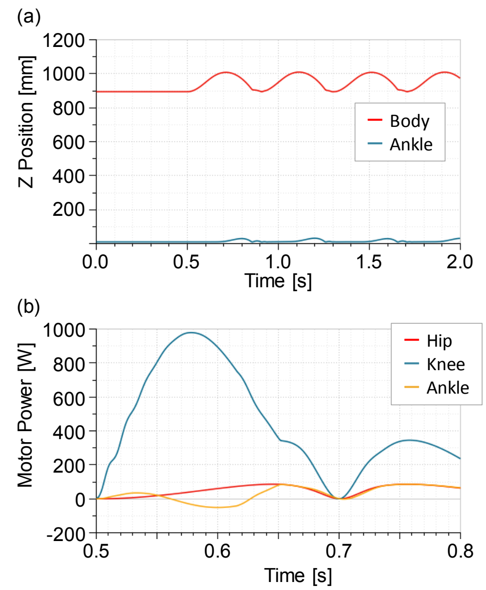

Figure 9. Simulation result: position and motor power. (a) Vertical position of the body and the ankle joint and (b) motor power of each joint at the first hop.

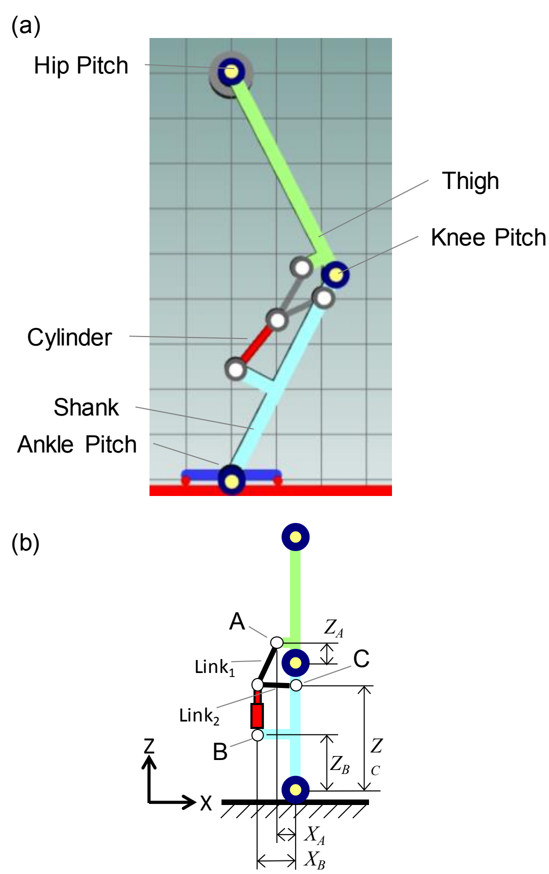

Figure 10. Four-bar-linkage mechanism: (a) link structure and (b) model parameters.

In this simulation, we assumed a mechanical transmission system as a conventional system, and the efficiency was set to 1 as an ideal condition. Thus, Figure 9 presents the simulation result, where it is apparent that the knee requires the highest motor power over the three axes, and the maximum power is 979 W.

B. Hydraulic Direct Drive System Model for Hopping

We developed the hydraulic direct drive system model for hopping to evaluate the effect of the proposed system. In this model, a motor was connected to the knee pitch joint, which requires the highest motor power in the leg joints via our proposed system. Other joints applied the conventional system.

The four-bar-linkage-mechanism was employed to secure a wide joint drive range with the cylinder. Figure 10 shows the mechanism, while 0lists the parameters.

Figure 11 shows the constructed hydraulic model, where Takako's pump [13] is modeled because it is small, and can be easily mounted. Figure 12 presents the pump efficiencies, and TABLE V lists the hydraulic model and control parametersTABLE V. The gains of the PD controller were obtained by trial and error to give a small target error for the joint angle.

The pump flow rate was limited when approaching the set relief pressure (i.e., 21 MPa) to reduce the loss by the relief flow when driving beyond the set pressure of the relief valve. The pump output power W_p is generally given by:

$$W_p = Q_{pump} P_p \tag{16}$$

where P_p is the output pressure of the pump. Similarly, the pump input power W_i is generally given by:

$$\mathrm{W_i} = \frac{\mathrm{W_p}}{\eta_{pv}\,\eta_{pm}} \tag{17}$$

where η_{pm} is the mechanical efficiency of the pump. A pump output power W_p of 979 W was required based on the simulation result in Figure 9. In addition, $\eta_{pv}\,\eta_{pm}$ was set to 0.8 based on Figure 12. Therefore, the pump output flow Q_{pump} could be determined from equations (16) and (17) for the pump output pressure P_p. Furthermore, the upper limit of the pump output flow Q_{pump} was set to 16 L/min. Figure 13 shows the installed relationship between the pump discharge pressure and the flow rate limit.

TABLE IV. PARAMETERS FOR THE FOUR-BAR-LINKAGE MECHANISM

Link$_1$ (mm)	119
Link$_2$ (mm)	113
X_A (mm)	59
Z_A (mm)	34
X_B (mm)	100
Z_B (mm)	200
X_C (mm)	0
Z_C (mm)	443

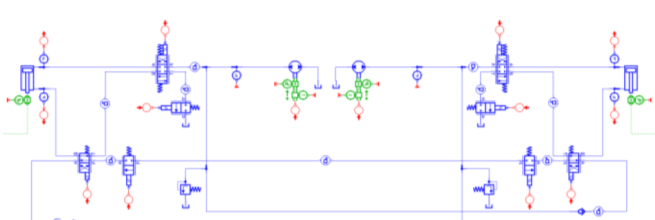

Figure 11. Hydraulic circuit model (LMS Amesim).

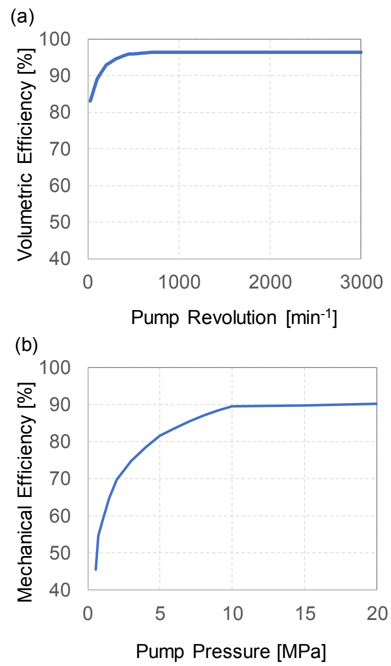

Figure 12. Pump efficiencies: (a) volumetric efficiency and (b) mechanical efficiency.

TABLE V. PARAMETERS FOR THE HYDRAULIC MODEL AND CONTROL

Pump displacement (cc/rev)	1.6
Pump relief pressure (MPa)	21
Cylinder stroke (mm)	132
Cylinder piston diameter (mm)	22
Cylinder rod diameter (mm)	10
Valves 1 and 3 pressure loss (MPa/(L/min))	0.1/50
Valve 2 maximum area (mm^2)	10
P gain	0.1
D gain	0.001

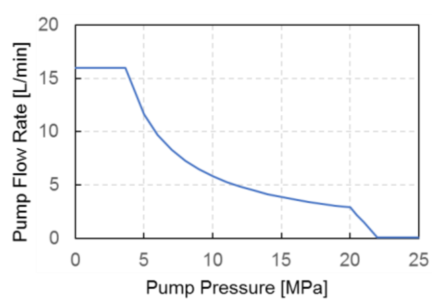

Figure 13. Pump P–Q limit.

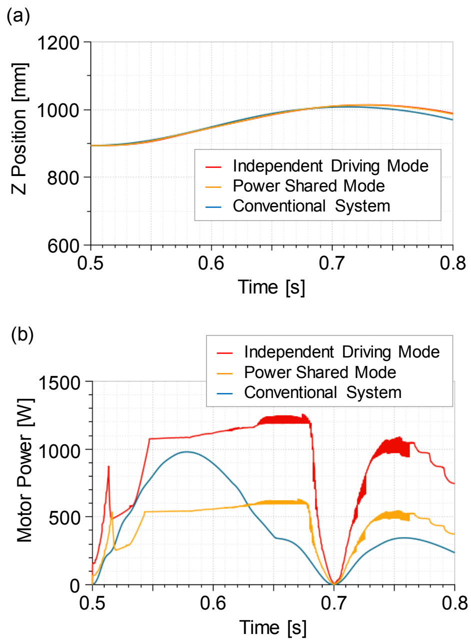

Figure 14. Result of the hydraulic direct drive system simulation. (a) The vertical position of the body, and (b) the motor power of each system.

C. Hopping Simulation of the Hydraulic Direct Drive System

In this simulation, we applied both the independent driving mode and the power shared driving mode. Figure 14 depicts the hopping simulation results. More specifically, Figure 14(a) shows that the independent driving mode and the power shared driving mode can realize the same hopping trajectory as the conventional system. The maximum power of the independent driving mode is 1260 W, and that of the power shared driving mode is 631 W. In the conventional system, the motor required a power of 979 W; hence, these results indicate that the maximum motor power can be reduced by 35.6% with the proposed power shared driving mode.

As previously mentioned, the power shared driving mode was also adopted in the simulation, allowing the power of the two pumps to be combined into a single cylinder. Furthermore, the pump efficiency and the pressure loss of the valve were considered. Therefore, the result of the maximum output being reduced to ~65% is reasonable. This result indicates that the required rated output of the motor can be reduced, such that smaller and lighter motors can be selected for installation into biped robots. For example, the axis that required a 1000 W motor in a conventional system requires only a 650 W motor in the case of our proposed system.

IV. Conclusions and Future Work

We proposed herein a hydraulic direct drive system of biped robots, which consisted of a combination of the independent drive mode and the power shared driving mode. In the independent drive mode, a cylinder was connected directly to one pump and controlled independently. In the power shared driving mode, two cylinders were driven in conjunction by linked pumps.

The simulation performed herein demonstrated that the power shared driving mode could reduce the required motor power by 35.6% while performing a hopping motion. This result suggests that the proposed system could allow downsizing of the motor driving the pump. This result is of relevance because of the issues related to space limitations in high-power and large electrical motors of conventional mechanical transmission systems.

Our future work will focus on the optimum method for obtaining the gains of the PD controller. The hydraulic direct drive system will also be applied to other axes. Furthermore, the proposed system will be applied to biped robots to perform walking, hopping, and running experiments. Moreover, we aim to develop seamless switching control between the independent drive mode and the power shared driving mode.

References

[1] Y. Ogura, K. Shimomura, H. Kondo, A. Morishima, T. Okubo, S. Momoki, H. O. Lim and A. Takanishi, “Human-like Walking with Knee Stretched, Heel-contact and Toe-off Motion by a Humanoid robot,” Proc. 2006 IEEE/RSJ Int. Conf. Intelligent Robots and Systems, pp. 3976–3981, 2006.

[2] T. Otani, K. Hashimoto, S. Hamamoto, S. Miyamae, M. Sakaguchi, Y. Kawakami, H.O. Lim and A. Takanishi, “Knee Joint Mechanism That Mimics Elastic Characteristics and Bending in Human Running,” Proc. 2015 IEEE/RSJ Int. Conf. Intelligent Robots and Systems, pp. 5156–5161, 2015.

[3] J. Urata, Y. Nakanishi, K. Okuda, and M. Inaba, “Design of High Torque and High Speed Leg Module for High Power Humanoid,” Proc. 2010 IEEE/RSJ Int. Conf. Intelligent Robots and Systems, pp. 4497–4502, 2010.

[4] Y. Ito, S. Nozawa, J. Urata, T. Nkaoka, K. Kobayashi, Y. Nakanishi, K. Okada, and M. Inaba “Development and verification of life-size humanoid with high-output actuation system,” Proc. 2014 IEEE Int. Conf. on Robotics and Automation, pp. 3433–3438, 2014.

[5] I. Park, J. Kim, J. Lee, and J. Oh, “Mechanical Design of the Humanoid Robot Platform, HUBO,” Advanced Robotics 21(11), pp. 1305–1322, 2007.

[6] Atlas | Boston Dynamics, https://www.bostondynamics.com/atlas, accessed 2018/09/10.

[7] S. Hyon, D. Suewaka, Y. Torii, and N. Oku, “Design and Experimental Evaluation of a Fast Torque-controlled Hydraulic Humanoid Robot,” Transactions on Mechatronics, 2017.

[8] H. Khan, S. Kitano, Y. Goa, D. G. Caldwell, C. Semini, “Development of the lightweight hydraulic quadruped robot—MiniHyQ”, Proc. IEEE Int. Conf. Technol. Practical Robot Appl., pp. 1–6, 2015.

[9] R. Rahmfeld, and M. Ivantysynova, “Energy Saving Hydraulic Actuators for Mobile Machines.” Proc. 1st Bratislavian Fluid Power Symposium, pp. 47–57, 1998.

[10] J. Zimmerman, E. Busquets, and M. Ivantysynova, “40% Fuel Savings by Displacement Control Leads to Lower Working Temperatures — A Simulation Study and Measurements,” Proc. the 52nd National Conference on Fluid Power, pp. 693–701, 2011.

[11] H. Kaminaga, J. Ono, Y. Nakashima, and Y. Nakamura, “Development of Backdrivable Hydraulic Joint Mechanism for Knee Joint of Humanoid Robots,” Proc. 2009 IEEE Int. Conf. on Robotics and Automation, pp. 1577–1582, 2009.

[12] Takako Industries, INC., http://www.takako-inc.com/, accessed 2018/09/10.